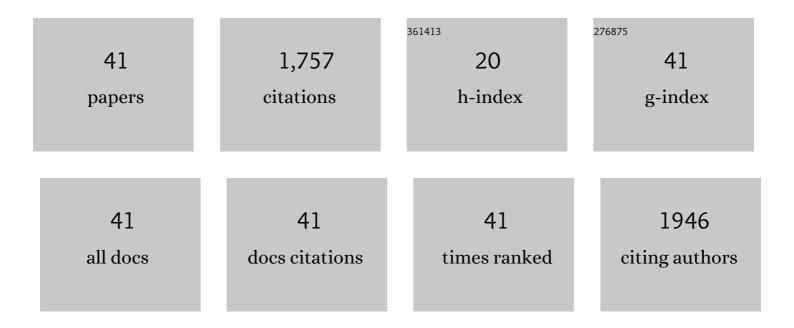
Jo-Anne Wartho

List of Publications by Year in descending order

Source: https://exaly.com/author-pdf/1865862/publications.pdf Version: 2024-02-01



#	Article	IF	CITATIONS
1	An (U-Th)/He age for the small Monturaqui impact structure, Chile. Quaternary Geochronology, 2022, 67, 101217.	1.4	1
2	Internal igneous growth, doming and rapid erosion of a mature ocean island: the Miocene evolution of Maio (Cabo Verde). International Journal of Earth Sciences, 2022, 111, 1129-1148.	1.8	1
3	Dendritic reidite from the Chesapeake Bay impact horizon, Ocean Drilling Program Site 1073 (offshore) Tj ETQq1	1 0.7843 4.4	14 _, rgBT /O
4	Origin of isolated seamounts in the Canary Basin (East Atlantic): The role of plume material in the origin of seamounts not associated with hotspot tracks. Terra Nova, 2020, 32, 390-398.	2.1	12
5	Paired EMI-HIMU hotspots in the South Atlantic—Starting plume heads trigger compositionally distinct secondary plumes?. Science Advances, 2020, 6, eaba0282.	10.3	26
6	(Uâ€Th)/He zircon dating of Chesapeake Bay distal impact ejecta from ODP site 1073. Meteoritics and Planetary Science, 2019, 54, 1840-1852.	1.6	6
7	40Ar-39Ar geochronology of the active phonolitic Cadamosto Seamount, Cape Verde. Lithos, 2019, 344-345, 464-481.	1.4	10
8	New Age and Geochemical Data from the Southern Colville and Kermadec Ridges, SW Pacific: Insights into the recent geological history and petrogenesis of the Proto-Kermadec (Vitiaz) Arc. Gondwana Research, 2019, 72, 169-193.	6.0	15
9	New age and geochemical data from the Walvis Ridge: The temporal and spatial diversity of South Atlantic intraplate volcanism and its possible origin. Geochimica Et Cosmochimica Acta, 2019, 245, 16-34.	3.9	40
10	Exploring the variability of argon loss in Apollo 17 impact melt rock 77135 using highâ€spatial resolution40Ar/39Ar geochronology. Meteoritics and Planetary Science, 2019, 54, 721-739.	1.6	4
11	Geology and palaeontology of the Hindon Maar Complex: A Miocene terrestrial fossil Lagerstäte in southern New Zealand. Palaeogeography, Palaeoclimatology, Palaeoecology, 2018, 500, 52-68.	2.3	14
12	Global distribution of the HIMU end member: Formation through Archean plume-lid tectonics. Earth-Science Reviews, 2018, 182, 85-101.	9.1	40
13	Unexpected HIMU-type late-stage volcanism on the Walvis Ridge. Earth and Planetary Science Letters, 2018, 492, 251-263.	4.4	34
14	Thermochronologic constraints on the slip history of the South Tibetan detachment system in the Everest region, southern Tibet. Earth and Planetary Science Letters, 2017, 459, 105-117.	4.4	32
15	Interaction of polar and tropical influences in the mid-latitudes of the Southern Hemisphere during the Mi-1 deglaciation. Global and Planetary Change, 2017, 155, 109-120.	3.5	7
16	Diachroneity of the Clearwater West and Clearwater East impact structures indicated by the (U–Th)/He dating method. Earth and Planetary Science Letters, 2016, 453, 56-66.	4.4	11
17	Age and structure of the Shyok suture in the Ladakh region of northwestern India: Implications for slip on the Karakoram fault system. Tectonics, 2015, 34, 2011-2033.	2.8	68
18	Refining lunar impact chronology through high spatial resolution ⁴⁰ Ar/ ³⁹ Ar dating of impact melts. Science Advances, 2015, 1, e1400050.	10.3	20

JO-ANNE WARTHO

#	Article	IF	CITATIONS
19	An integrated sequence stratigraphic and chronostratigraphic analysis of the Pliocene, Tiburon Basin succession, Mejillones Peninsula, Chile. Global and Planetary Change, 2015, 131, 124-147.	3.5	1
20	Dating the cooling of exhumed central uplifts of impact structures by the (U–Th)/He method: A case study at Manicouagan. Chemical Geology, 2014, 377, 56-71.	3.3	21
21	Postcollisional High-Grade Metamorphism, Orogenic Collapse, and Differential Cooling of the East African Orogen of Northeast Mozambique. Journal of Geology, 2012, 120, 507-530.	1.4	24
22	An (Uâ€Th)/He age for the shallowâ€marine Wetumpka impact structure, Alabama, USA. Meteoritics and Planetary Science, 2012, 47, 1243-1255.	1.6	12
23	Post Pan-African thermo-tectonic evolution of the north Mozambican basement and its implication for the Gondwana rifting. Inferences from ⁴⁰ Ar/ ³⁹ Ar hornblende, biotite and titanite fission-track dating. Geological Society Special Publication, 2009, 324, 261-286.	1.3	18
24	Proterozoic deformation in the northwest of the Archean Yilgarn Craton, Western Australia. Precambrian Research, 2008, 162, 354-384.	2.7	28
25	Early history of the eastern Sibao Orogen (South China) during the assembly of Rodinia: New mica 40Ar/39Ar dating and SHRIMP U–Pb detrital zircon provenance constraints. Precambrian Research, 2007, 159, 79-94.	2.7	275
26	Magmatic Evolution and Ascent History of the Aries Micaceous Kimberlite, Central Kimberley Basin, Western Australia: Evidence from Zoned Phlogopite Phenocrysts, and UV Laser 40Ar/39Ar Analysis of Phlogopite–Biotite. Journal of Petrology, 2006, 47, 1751-1783.	2.8	47
27	A chronology of foreland deformation: ultra-violet laser 40Ar/39Ar dating of syn/late-orogenic intrusions from the Variscides of southwest Ireland. Journal of Structural Geology, 2005, 27, 1413-1425.	2.3	23
28	Estimates of Ar diffusion and solubility in leucite and nepheline: Electron microprobe imaging of Ar distribution in a mineral. American Mineralogist, 2005, 90, 954-962.	1.9	8
29	Time Markers for the Evolution and Exhumation History of a Late Palaeozoic Paired Metamorphic Belt in North–Central Chile (34°–35°30′S). Journal of Petrology, 2005, 46, 1835-1858.	2.8	102
30	Laser 40Ar/39Ar ages of single detrital white mica grains related to the exhumation of Neoproterozoic and Late Devonian high pressure rocks in the Southern Urals (Russia). Geological Magazine, 2004, 141, 161-172.	1.5	13
31	40Ar–39Ar dating of detrital muscovite in provenance investigations: a case study from the Adelaide Rift Complex, South Australia. Earth and Planetary Science Letters, 2004, 227, 297-311.	4.4	46
32	The â€~zero charge' partitioning behaviour of noble gases during mantle melting. Nature, 2003, 423, 738-741.	27.8	107
33	Origin and Migration of the Alpine Iceman. Science, 2003, 302, 862-866.	12.6	229
34	⁴⁰ Ar/ ³⁹ Ar ages in mantle xenolith phlogopites: determining the ages of multiple lithospheric mantle events and diatreme ascent rates in southern Africa and Malaita, Solomon Islands. Geological Society Special Publication, 2003, 220, 231-248.	1.3	14
35	Ar and K partitioning between clinopyroxene and silicate melt to 8 GPa. Geochimica Et Cosmochimica Acta, 2002, 66, 507-519.	3.9	58
36	Rapid Kimberlite Ascent and the Significance of Ar-Ar Ages in Xenolith Phlogopites. Science, 2000, 289, 609-611.	12.6	172

JO-ANNE WARTHO

#	Article	IF	CITATIONS
37	Direct measurement of Ar diffusion profiles in a gem-quality Madagascar K-feldspar using the ultra-violet laser ablation microprobe (UVLAMP). Earth and Planetary Science Letters, 1999, 170, 141-153.	4.4	100
38	Preliminary UVLAMP determinations of argon partition coefficients for olivine and clinopyroxene grown from silicate melts. Chemical Geology, 1998, 147, 185-200.	3.3	41
39	Photo-emission electron microscopy (PEEM) heating investigations of a natural amphibole sample. Mineralogical Magazine, 1995, 59, 121-127.	1.4	9
40	Apparent argon diffusive loss 40Ar/39Ar age spectra in amphiboles. Earth and Planetary Science Letters, 1995, 134, 393-407.	4.4	33
41	Disturbed 40Arî—,39Ar spectra from hornblendes: Thermal loss or contamination. Chemical Geology, 1993, 103, 271-281.	3.3	28